



## Sheared Iherzolite xenoliths revisited

Philip Skemer<sup>1,2</sup> and Shun-ichiro Karato<sup>2</sup>

Received 22 July 2007; revised 15 February 2008; accepted 11 March 2008; published 19 July 2008.

[1] The microstructures of sheared Iherzolite xenoliths from South African kimberlites are investigated using new microstructural analysis techniques and new rheological data. By applying electron backscatter diffraction (EBSD) methods and the M-index technique for quantifying the strength of lattice preferred orientation (LPO), it is demonstrated that olivine and orthopyroxene, after an initial stage of dynamic recrystallization, deformed by different mechanisms: olivine deformed by dislocation creep, while orthopyroxene deformed by a grain-size sensitive mechanism that randomized the preexisting LPO. New rheological data, which incorporate the effects of pressure on deformation, are applied to these xenoliths. The effects of pressure are shown to dramatically reduce the inferred strain rates of these xenoliths in comparison to previous estimates. The contrasting microstructural features of olivine and orthopyroxene are analyzed using the Avrami theory of recrystallization, coupled with microstructural observations and experimental data. This analysis suggests that (1) the difference in the recrystallized grain-size and (2) the difference in the completeness of recrystallization, can be largely explained by the contrast in grain boundary mobility between olivine and orthopyroxene.

**Citation:** Skemer, P., and S.-i. Karato (2008), Sheared Iherzolite xenoliths revisited, *J. Geophys. Res.*, 113, B07205, doi:10.1029/2007JB005286.

### 1. Introduction

[2] Peridotite xenoliths have long been known to record valuable information about deformation processes in the upper mantle [e.g., Mercier and Nicolas, 1975; Boullier and Nicolas, 1975]. Kimberlite xenoliths, in particular, may be exhumed from depths in excess of 200 km [e.g., Boyd, 1973]. As such, the deformation microstructures they record may contain information about deformation processes at the base of the continental lithosphere. Often, the deepest kimberlite xenoliths have been severely deformed, developing a fluidal microstructure of recrystallized olivine and orthopyroxene similar to microstructures observed in crustal mylonites [Boullier and Gueguen, 1975]. While these highly deformed peridotites have been extensively studied from a variety of perspectives [Boullier and Gueguen, 1975; Nixon et al., 1973; Green and Gueguen, 1974; Goetze, 1975; Boyd and Nixon, 1975; Ehrenberg, 1979; Mercier, 1979; Kennedy et al., 2002], there are still many unanswered questions about the significance of these microstructures, and what they can tell us about deformation at the base of continents and other geologically inaccessible regions of the upper mantle.

[3] Although both olivine and orthopyroxene show evidence of dynamic recrystallization, aspects of their microstructures are quite different, particularly the recrystallized

grain-size and the degree of recrystallization. Because of these and other microstructures, previous studies have argued that the recrystallized orthopyroxene deformed by grain-size sensitive creep while the recrystallized olivine deformed by dislocation creep [Boullier and Gueguen, 1975; Gueguen and Boullier, 1976]. This implies that deformation might become localized in the fine-grained orthopyroxene bands, and that under some circumstances orthopyroxene may become weaker than olivine. This is an intriguing observation, as it contradicts the paradigm that olivine is weaker than orthopyroxene, and therefore controls the rheology of the upper mantle [e.g., Karato and Wu, 1993; Hirth and Kohlstedt, 2003]. However, in none of the previous studies was the cause for the contrasting microstructures of olivine and orthopyroxene explained. Therefore the significance of these observations to the broader geological context is unknown.

[4] In this study we have applied the SEM-based observation technique of electron backscatter diffraction (EBSD) [e.g., Randle, 2003] to analyze the microstructures of the sheared Iherzolites. These microstructural observations are evaluated using a new method for quantifying the strength of the lattice-preferred orientation (LPO) [Skemer et al., 2005] to better infer the deformation mechanisms of olivine and orthopyroxene. By employing new rheological data we have estimated the strain rates achieved by these samples. Using the Avrami theory of recrystallization [Avrami, 1939], coupled with microstructural observations and experimental data on grain-boundary mobility [Karato, 1989; Skemer and Karato, 2007], we have provided a plausible explanation for the contrasting behavior of olivine and orthopyroxene. Finally, we discuss the possible implications of these

<sup>1</sup>Department of Geosciences, Brown University, Providence, Rhode Island, USA.

<sup>2</sup>Department of Geology and Geophysics, Yale University, New Haven, Connecticut, USA.

observations for the deformation of the upper mantle in general.

## 2. Sample and Microstructural Description

[5] We studied four mantle xenoliths from the Jagersfontein kimberlite that exhibit mosaic textures (*sensu* [Boullier and Nicolas, 1975]). Detailed descriptions of these samples are given by Boyd and Mertzman [1987]. Petrologically, these samples are garnet-bearing lherzolites (Ol+Opx+Cpx+Gt). Serpentine is abundant along olivine grain boundaries. Equilibrium temperatures and pressures were calculated by F. R. Boyd (personal communication, 2001) using the two-pyroxene thermometry and Al-in-opx barometry calibrations of Brey and Koehler [1990]. These results ( $T \sim 1600\text{--}1640\text{ K}$  and  $P \sim 5.5\text{--}5.8\text{ GPa}$ ) indicate that the last chemical equilibration with respect to these particular elements occurred at depths of approximately 200 km.

[6] Hand samples are massive and exhibit no obvious fabric elements. Samples were oriented with respect to the microstructural features by cutting orthogonal thin sections and by examining polished surfaces under a low power stereo microscope. In thin section, bands of orthopyroxene grains form a laminar, often interconnected microstructure, which defines both a foliation and a lineation within the foliation. There are two populations of orthopyroxene grains. The smaller orthopyroxene grains form the majority of the bands, and are frequently seen on the margins of a few, remnant, larger grains (Figure 1). This microstructure is readily interpreted as the product of dynamic recrystallization, with large porphyroclasts being broken down into bands of fine-grained neoblasts [e.g., Passchier and Trouw, 1998]. The length of the orthopyroxene bands varies from 1 mm to >10 mm with widths between 100  $\mu\text{m}$  and 1 mm, when measured in a section normal to the foliation and parallel to the lineation. The recrystallized grain-size is 33–54  $\mu\text{m}$  (Table 1), where grain-size is determined using the mean intercept technique, with a sectioning correction factor of 1.5 applied to account for the intersection of a 2D section through 3D grains. Most orthopyroxene neoblasts have a nearly equant morphology with straight grain boundaries (Figure 1e). The remnant porphyroclasts show infrequent subgrain boundaries (as observed by optical microscopy), with a subgrain spacing ( $\sim 200\text{--}400\ \mu\text{m}$ ) that is significantly larger than the size of the neoblasts (Figure 1d). Olivine grains form an equant matrix with minor shape-preferred orientation. Rare remnant porphyroclasts in our samples, coupled with the range of porphyroclastic microstructures found in other kimberlite xenoliths [Boullier and Nicolas, 1975] indicate that the olivine is completely recrystallized. The olivine recrystallized grain sizes range from 157–340  $\mu\text{m}$ . In some samples garnets are slightly elongated parallel to the orthopyroxene lineation. Clinopyroxene is deformed but rarely recrystallized, and represents a small volume fraction of the samples.

## 3. Deformation Mechanisms

[7] One of the most notable features of the sheared lherzolite xenoliths is the contrast in recrystallized grain-size between olivine and orthopyroxene. This contrasting behavior is not normally seen in alpine-type massifs or

shallower xenoliths [e.g., Nicolas *et al.*, 1971; Mercier and Nicolas, 1975], but may have important mechanical consequences. Depending on the conditions of deformation, a reduction in grain size by dynamic recrystallization may cause a material to undergo a transition from dislocation creep to grain-size sensitive creep, resulting in a weakening of the material [Twiss, 1976; Rutter and Brodie, 1988; de Bresser *et al.*, 1998, 2001]. Typically it is assumed that dislocation creep and grain-size sensitive creep can be distinguished using the presence or absence of lattice-preferred orientation (LPO), respectively [e.g., Karato *et al.*, 1995; Fliervoet *et al.*, 1999; Warren and Hirth, 2006]. However, some experimental results [Rutter *et al.*, 1994; Gomez Barreiro *et al.*, 2007] suggest that this relationship may not be straightforward, particularly when deformation occurs near a regime boundary on a deformation mechanism map (i.e., when deformation is accommodated by more than one mechanism). In this study we will assume that strong LPO corresponds to deformation in the dislocation creep regime, while random LPO or the destruction of LPO corresponds to deformation in a grain-size sensitive regime, far from any regime boundary.

[8] This assumption was also made in earlier microstructural studies of sheared lherzolite xenoliths [Boullier and Gueguen, 1975; Gueguen and Boullier, 1976], in which the authors proposed that a transition to grain-size sensitive creep may have occurred during deformation of the orthopyroxene. Using a universal stage microscope, the authors measured the LPO of 100 orthopyroxene neoblasts, scattered throughout the sample. On the basis of a qualitative evaluation of the data, the authors concluded that the fabric was random and that the orthopyroxene must have deformed by a grain-size sensitive mechanism. While this observation is intriguing, the methodology and the small number of data are not totally satisfactory. Thus we have revisited this question using a number of new techniques.

[9] In our study the LPO of the olivine and orthopyroxene neoblasts was measured using electron backscatter diffraction (EBSD), an SEM based technique with considerably higher spatial and angular resolution and more rapid data acquisition than a universal stage microscope [Randle, 2003]. The strength of the fabrics was determined quantitatively using the newly developed M-index technique [Skemer *et al.*, 2005]. In the M-index technique, the distribution of a sample's random-pair misorientation angles [Wheeler *et al.*, 2001] is compared to a distribution of misorientation angles from a theoretical random fabric. The M-index is scaled from zero to one, where  $M = 0$  represents a random fabric and  $M = 1$  represents a single crystal. Using this technique, quantitative estimates of fabric strengths can be obtained for as few as  $\sim 150$  grains. EBSD analyses were performed on thin-sections prepared parallel to the lineation and perpendicular to the foliation, as defined by the flattening and elongation of orthopyroxene bands. EBSD patterns were indexed manually using Channel 5+ software by HKL Technologies. An accelerating voltage of 20 kV and a beam current of 2.4 nA were used at a working distance of 20 mm. Olivine neoblast orientations were collected in a grid with spacing that was roughly twice the mean grain-size to ensure that individual grains were not over-sampled. Orthopyroxene bands were analyzed individually. Because we are interested in observing the evolution

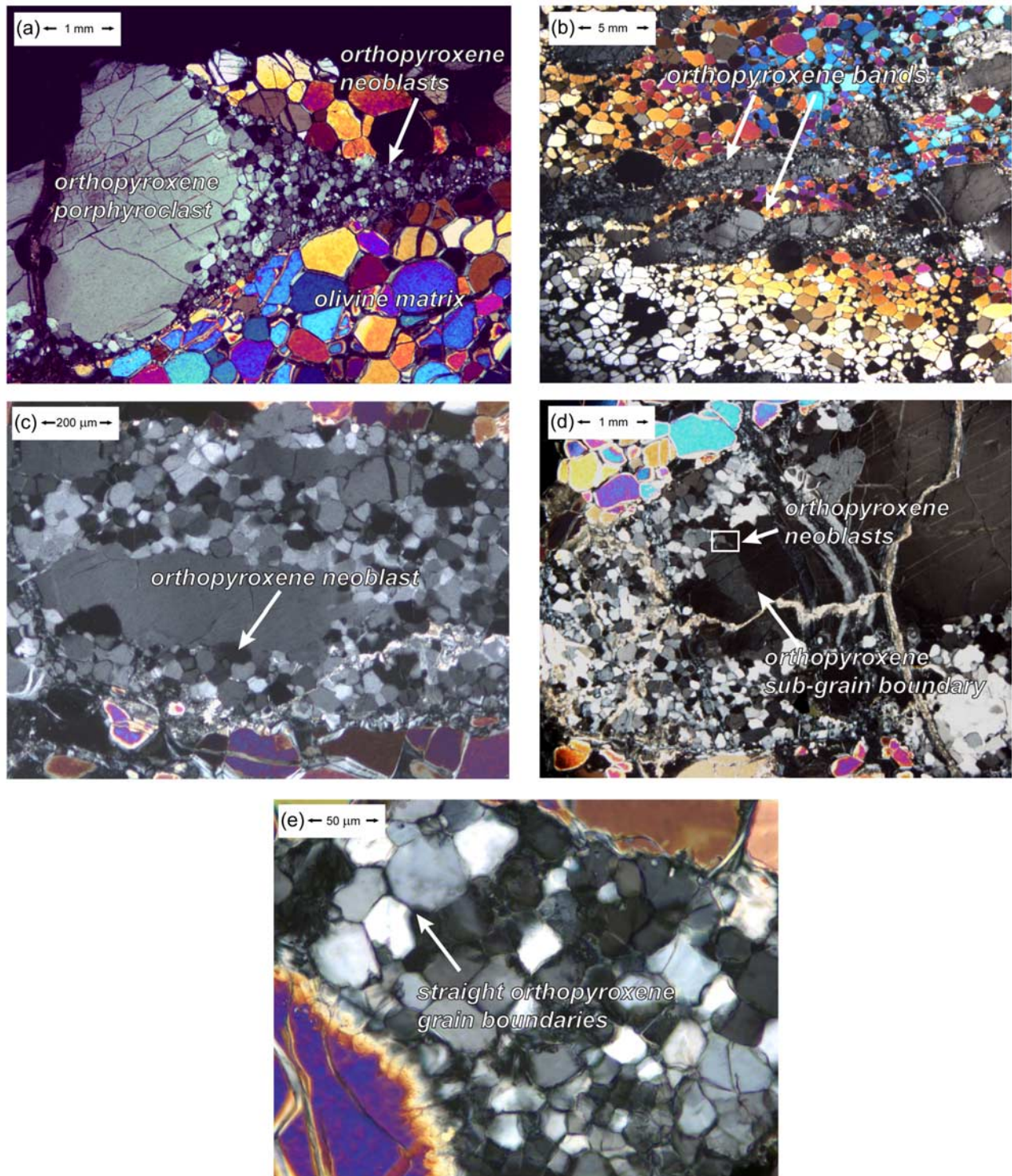


**Figure 1.** Photomicrographs of the orthopyroxene and olivine microstructures. (a) A large orthopyroxene porphyroclast, left, is recrystallizing into a band of fine-grained neoblasts. Olivine forms an equigranular mosaic of larger, recrystallized grains. (b) A coarse scale image of several orthopyroxene bands transecting a sample. (c) Neoblasts forming at the margin of a porphyroclast. (d) The subgrain microstructure of an orthopyroxene porphyroclast. The subgrain spacing is considerably larger than the recrystallized grain size. The boxed region highlights neoblasts forming on a subgrain boundary. (e) A higher magnification image showing orthopyroxene grain boundaries.

**Table 1.** Summary of Grain-Size and Grain Size Piezometry

| Sample                 | Opx Recrystallized Grain Size, $\mu\text{m}$ | Olivine Recrystallized Grain Size, $\mu\text{m}$ | Deviatoric Stress, MPa |
|------------------------|--|--|------------------------|
| FRB 997c               | $54 \pm 7$                                   | $309 \pm 44$                                     | $18 \pm 2$             |
| FRB 1003a              | $35 \pm 5$                                   | $157 \pm 26$                                     | $30 \pm 5$             |
| FRB 1031               | $37 \pm 5$                                   | $340 \pm 67$                                     | $17 \pm 3$             |
| FRB 1033               | $48 \pm 8$                                   | $245 \pm 32$                                     | $22 \pm 2$             |
| JAG 90-68 <sup>a</sup> | $33 \pm 6$                                   | $190 \pm 30$                                     | $27 \pm 3$             |
| BG1975 <sup>b</sup>    | $10 \pm 2$                                   | $70 \pm 15$                                      | $57 \pm 10$            |

<sup>a</sup>*Jin* [1995].<sup>b</sup>*Boullier and Gueguen* [1975].

of orthopyroxene LPO with progressive strain, bands were only analyzed when there was an obvious parent-daughter relationship between the porphyroblast and the neoblasts. Most porphyroblast-neoblast clusters did not meet this

criterion, as they are often interconnected with other recrystallizing orthopyroxene bands.

[10] In all samples studied, the olivine [100] axes are aligned subparallel to the sample lineation and the [010] axes are aligned subnormal to the foliation (Figure 2). This pattern is an example of the A-type fabric, consistent with deformation on the [100](010) slip system). This particular LPO forms at high temperature, low stress, and water-poor conditions [*Jung and Karato, 2001a*].

[11] The orthopyroxene porphyroclasts display various degrees of recrystallization. In most cases some of the porphyroclast remains unrecrystallized. Neoblasts are found along the margins of the porphyroclast (Figures 1a and 1c) or along subgrain boundaries (Figure 1d). In some cases recrystallization may be more complete and the porphyroclast may be largely consumed. In many cases, the

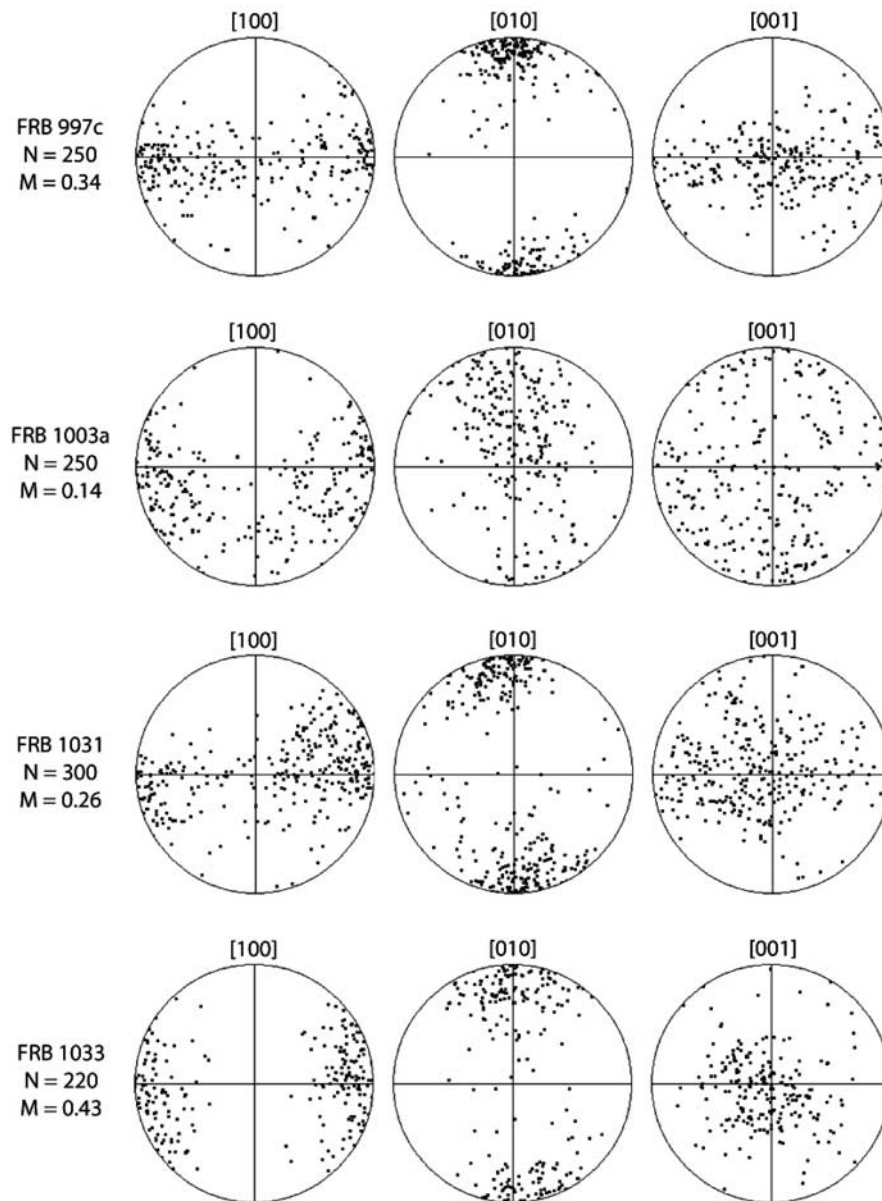


**Figure 2.** Lattice-preferred orientation of olivine. Pole figures are plotted for each sample with the lineation E-W and the pole to the foliation N-S.  $N$  is the number of grains in the analysis.  $M$  is the M-index quantification of fabric strength. All fabrics show an A-type symmetry, and have moderate to large  $M$  indices.

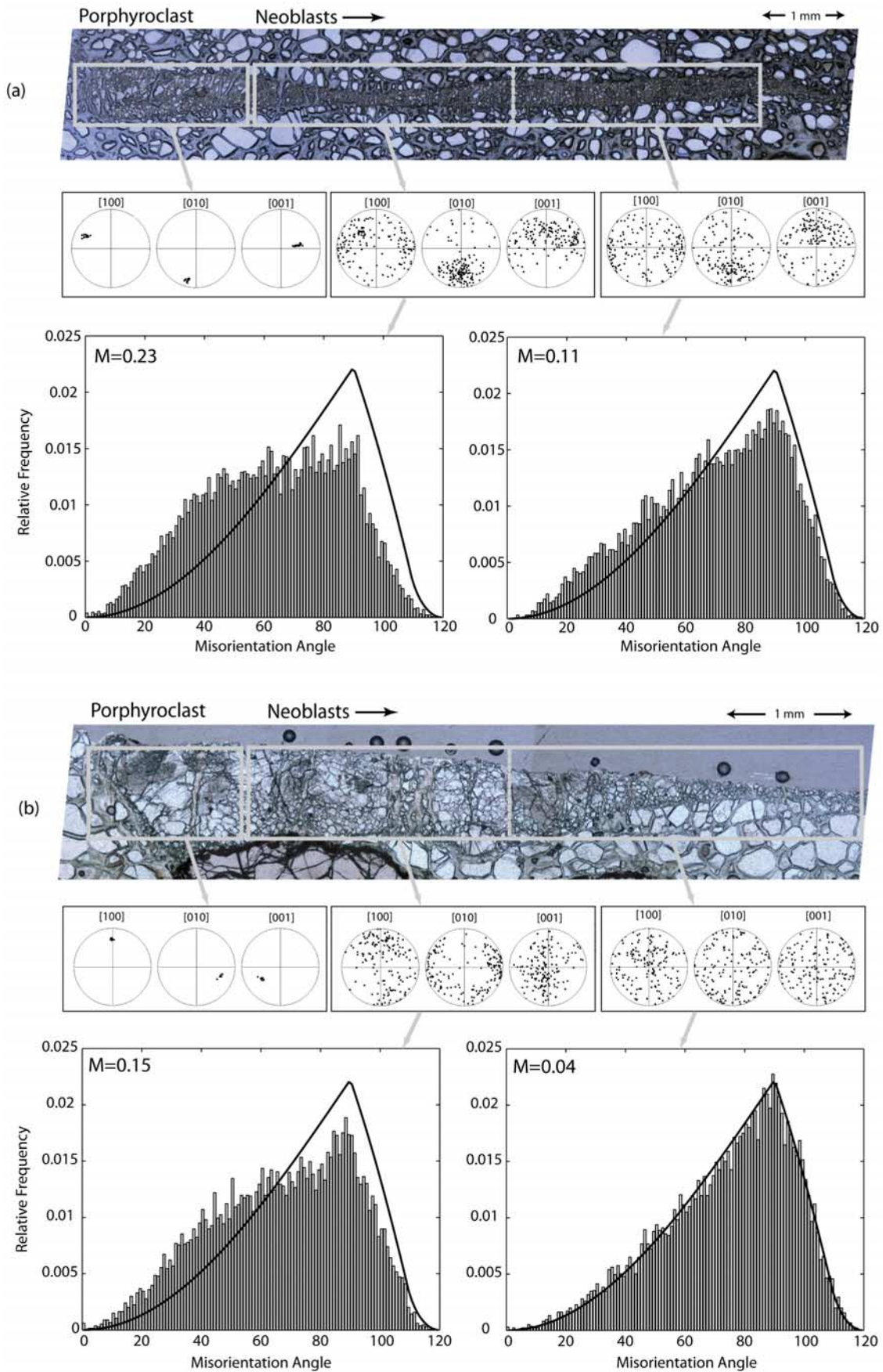


Figure 3

**Table 2.** Previous Strain-Rate Estimates

| Study                        | Flow-Law Applied                 | Stress, MPa          | Strain Rate, 1/s |
|------------------------------|----------------------------------|----------------------|------------------|
| Goetze [1975]                | Kohlstedt and Goetze [1974]      | 200–300 <sup>a</sup> | 3 E-04           |
| Mercier [1979]               | Post and Griggs [1973]           | 200–300 <sup>b</sup> | 1 E-08           |
| Kennedy <i>et al.</i> [2002] | Chopra and Paterson [1984] “wet” | 40–150 <sup>c</sup>  | 1 E-05           |

<sup>a</sup>Dislocation density [Kohlstedt and Goetze, 1974].

<sup>b</sup>Olivine grain-size [Mercier *et al.*, 1977; Ross *et al.*, 1980].

<sup>c</sup>Olivine grain-size [Van der Wal *et al.*, 1993].

orientation of an individual porphyroclast is deviated from the “ideal” orientation expected of mantle-deformed orthopyroxene, which deforms almost exclusively on the [001](100) slip-system [e.g., Christensen and Lundquist, 1982]. Even in these cases, the maxima of the neoblast LPO (if any LPO is present) is similar to the orientation of the parent porphyroclast. Instead of rotating toward the orientation prescribed by the dominant slip system and deformation geometry, as would be expected during dislocation creep, the LPO of the neoblasts becomes progressively more diffuse around the orientation of the porphyroclast. This is strong evidence that the LPO of the neoblasts is inherited rather than formed by subsequent deformation, and that dislocation creep does not contribute significantly to the overall deformation process [cf. Bestmann and Prior, 2003; Storey and Prior, 2005; Halfpenny *et al.*, 2006].

[12] In the more highly deformed bands (bands with aspect ratios greater than  $\sim 3$ ) it is possible to observe the progressive obliteration of the fabric initially acquired from the porphyroclast. This progressive randomization is recognized quantitatively by a decreasing M-index. Figure 3 illustrates this phenomenon in two highly deformed bands: In Figure 3a the 161 neoblasts closest to the porphyroclast have a misorientation index of  $M = 0.23$ , while the 160 neoblasts further away from the porphyroclast have a misorientation index of  $M = 0.11$ . In Figure 3b the 165 neoblasts closest to the porphyroclast have a misorientation index of  $M = 0.15$ , while the 164 neoblasts further away from the porphyroclast have a misorientation index of  $M = 0.04$ . This progressive weakening of the fabric with increasing strain is a strong indication that deformation, subsequent to recrystallization, was accommodated by diffusion creep or another grain-size sensitive mechanism that involves grain-boundary sliding.

## 4. Strain Rate

### 4.1. Previous Investigations

[13] An important constraint on the significance of sheared lherzolite xenoliths is the strain rate attained during deformation. A number of authors have attempted this calculation with markedly different results (Table 2). In an earlier analysis of this problem, [Goetze, 1975] determined that olivine strain rates were on the order of  $\sim 10^{-4} \text{ s}^{-1}$ , and

concluded that these xenoliths recorded only a very short-lived geologic event, probably associated with the kimberlite eruption. A contemporary study by [Mercier, 1979] determined lower strain rates ( $\sim 10^{-8} \text{ s}^{-1}$ ) but drew similar conclusions regarding the xenoliths’ origins. A more recent study by [Kennedy *et al.*, 2002] determined olivine strain rates of  $\sim 10^{-5} \text{ s}^{-1}$  for similar high temperature xenoliths. The variation in these estimates is largely attributable to the fact that each study employed different calibrations for the stress estimate, and different flow laws for the strain rate calculation (Table 2). A significant shortcoming of all of these calculations is that they do not account for the effects of pressure on the calculated strain rates. The effects of water are also poorly constrained. Experimental data on olivine rheology has demonstrated the importance of these two effects [e.g., Karato and Jung, 2003; Mei and Kohlstedt, 2000]. Here, we will revisit this issue using the newest rheological data, which explicitly accounts for the effects of water content and pressure effects on strain rate.

### 4.2. Conditions of Deformation

[14] The strain rate attained by a sample during steady state dislocation creep is largely a function of water content ( $C_{\text{OH}}$ ), stress ( $\sigma$ ), temperature (T), and pressure (P) [e.g., Poirier, 1985].

[15] The A-type olivine LPO observed in these samples provides some constraint on the water content present during deformation. Given the available data, the A-type olivine LPO is thought to form only at water-poor conditions ( $< 200$  ppm H/Si, assuming the [Paterson, 1982] calibration for water in olivine is applied) [Katayama *et al.*, 2004]. At higher water contents, one would expect to find the olivine E- or C-type LPOs. Even at these low levels, the presence of water may have a modest effect on rheology. Because of limitations of the rheological data for orthopyroxene (see below) we will apply “dry” flow laws in our subsequent analysis. However, if the maximum amount of water (200 ppm H/Si) is present, strain rates in olivine may be higher by as much as one order of magnitude [Mei and Kohlstedt, 2000].

[16] Stress may be inferred from the dynamically recrystallized grain-size. In this study we apply the dynamically recrystallized grain-size piezometer of [Karato *et al.*, 1980]. This piezometer does not explicitly account for the

**Figure 3.** Progressive randomization of orthopyroxene lattice-preferred orientation in individual, isolated bands. Two examples are shown (a,b). In the photomicrographs, the porphyroclasts are on the left, and the neoblasts are extending out to the right. Pole figures of different sections of the band show that the maxima of the neoblasts’ LPO is similar to the orientation of the associated porphyroclasts, indicating that the fabric is derived rather than produced by subsequent deformation. Histograms of random-pair misorientation angles for each set of neoblasts are plotted; the solid line is the theoretical distribution of misorientation angles for a random fabric.  $M$  is the M-index. The decreasing M-index with distance from the porphyroclast is indicative of the progressive randomization of the orthopyroxene LPO with increasing strain.

effects of pressure and temperature. However, experiments conducted over a large range of homologous temperatures ( $T/T_m = 0.63-0.88$ ) do not show any significant variation in the recrystallized grain-size versus stress relationship [Karato *et al.*, 1980; van der Wal *et al.*, 1993; Jung and Karato, 2001b]. The influence of water on recrystallized grain-size is also small for water contents less than  $\sim 100$  ppm H/Si, as inferred from a comparison of the results [Karato *et al.*, 1980; van der Wal *et al.*, 1993]. The xenoliths, according to our estimates, were deformed at  $T/T_m$  of 0.67 (see below) and at relatively dry conditions, within the range of the experimental calibrations. Therefore the use of this piezometer is justified. The dynamically recrystallized grain size of olivine, in the samples studied here, ranges from 157–340  $\mu\text{m}$  (Table 1). These grain-sizes correspond to stresses on the order of 17–30 MPa. A sample analyzed by Jin [1995] had comparable grain-sizes. The study by Boullier and Gueguen [1975] observed somewhat smaller recrystallized grains ( $\sim 70$   $\mu\text{m}$ ), consistent with a stress of 57 MPa.

[17] Stress may also be inferred from the dislocation density ( $\rho$ ), as:

$$\rho \cong \frac{1}{b^2} \left( \frac{\sigma}{\mu} \right)^m \quad (1)$$

where  $b$  is the length of the Burgers vector,  $\mu$  is the shear modulus, and  $m$  is a constant of order 1.4 [e.g., Karato and Jung, 2003]. This piezometer was calibrated at high temperature (1473–1573 K) and relatively low pressure ( $P = 0.3$  GPa). However, over the range of the conditions of interest, the relationship is only weakly dependent on pressure via the pressure dependence of the shear modulus, which increases by only  $\sim 10\%$  from 0.3 to 5.5 GPa. We measured the olivine neoblast dislocation density using an SEM based technique (see Karato [1987] for details) and found dislocation densities of  $1-2 \times 10^{11} \text{ m}^{-2}$ , which corresponds to stresses of 25–40 MPa. Jin [1995] reported comparable dislocation densities. Gueguen and Boullier [1976] report olivine dislocation densities in the range of  $1-5 \times 10^{11} \text{ m}^{-2}$ , corresponding to stresses of 25–70 MPa.

[18] In order to interpret the stress determined by the grain-size and dislocation density piezometers,  $\sigma(d)$  and  $\sigma(\rho)$  respectively, we must confirm that the xenoliths' microstructures correspond to "steady state" deformation. Deformation microstructures may be altered in two ways: by static annealing or by a subsequent transient stress pulse. During static annealing, microstructural alteration occurs through the recovery of energy stored as dislocations and grain-boundaries. At the conditions experienced by the xenoliths, the characteristic time for dislocation annihilation is  $\tau_{da} \sim 1 \times 10^6$  s and the characteristic time for grain-growth is  $\tau_{gg} \sim 7 \times 10^7$  s [cf. Toriumi and Karato, 1978; Karato and Ogawa, 1982; Karato, 1989]. Since the rate of dislocation annihilation is considerably faster than the rate of grain-growth, an annealing event would be recognized by  $\sigma(\rho) < \sigma(d)$ . A transient stress pulse would, on the other hand, be recognized by  $\sigma(\rho) > \sigma(d)$ , since steady state dislocation microstructures are formed after the accumulation of only a few percent strain [Durham *et al.*, 1977], while grain-size alteration by dynamic recrystallization requires at least 10% strain [e.g., Karato *et al.*, 1980; van der Wal *et al.*, 1993]. In Figure 4, we plot dislocation density versus grain-size for

each sample listed in Table 1. All samples fall, within error, on the line corresponding to the steady state relationship between dislocation density and grain-size. Thus we conclude that there was no significant alteration of the deformation microstructures post deformation.

[19] As noted above, the four samples from Jagersfontein (samples labeled "FRB" in Table 1), exhibit a fairly narrow range of equilibrium temperatures and pressures. We have assumed typical values  $T = 1623$  K and  $P = 5.5$  GPa for all subsequent calculations. No P-T information are available for the two data points obtained from the literature [Boullier and Gueguen, 1975, Table 1; Jin, 1995], so we will assume that the equilibrium P-T conditions are comparable for all six samples. In the subsequent analysis, we make the assumption that the temperature and pressure of chemical equilibration are the same as the temperature and pressure of deformation. This is often not the case, as a sample may be chemically re-equilibrated at different P-T conditions after deformation has ceased. However, in these samples there is strong evidence to suggest that the equilibrium P-T conditions are close to the deformation conditions. First, there is little evidence of static recovery; as noted above, all data fall on the steady state relationship between grain-size and dislocation density. Furthermore, all of the data plot above the contour for a  $10^7$ s annealing event (Figure 4). This indicates that if any annealing or static transport occurred, it must have lasted for less than  $10^7$ s. Given the diffusivity of calcium in orthopyroxene and the size of the orthopyroxene porphyroclasts, complete chemical re-equilibration of calcium would require approximately  $10^{10}$  s [Huebner and Voigt, 1984]. Thus we conclude that there was insufficient time for the xenoliths to experience static transport and subsequent re-equilibration at different P-T conditions. A similar argument can be made by looking at the composition of the orthopyroxene porphyroclasts and neoblasts: For one particular sample, we measured the CaO content at the center of a porphyroclast and the CaO content at the center of several associated neoblasts. Within the detection limits of the microprobe, the calcium contents were the same ( $\sim 0.95$  wt. %). The solubility of calcium in orthopyroxene is strongly temperature dependent, so if the neoblasts formed at a different temperature than the porphyroclast, we would expect the two to have different calcium contents. Applying the calcium-in-orthopyroxene calibration of [Brey and Koehler 1990], and taking into account the approximate resolution of the analytical technique ( $\sim 0.05$  wt. %) we conclude that the neoblasts formed at temperatures within about 30 K of the "equilibrium" temperature determined from the porphyroclast. Together, these two lines of evidence indicate that no substantial change in temperature or pressure occurred during or after the deformation process. Thus the use of the equilibrium thermobarometry to infer the deformation pressure and temperature is justified.

#### 4.3. Olivine Strain Rate

[20] Olivine strain rates were calculated using the flow law parameters of Karato and Jung [2003] using a standard constitutive law:

$$\dot{\epsilon} = A\sigma^n \exp\left(-\frac{E^* + PV^*}{RT}\right) \quad (2)$$

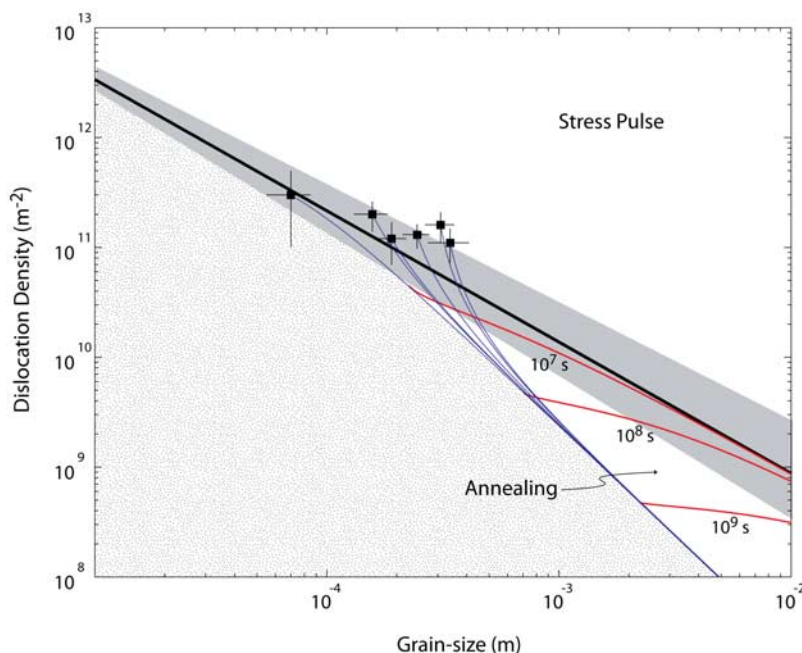


**Figure 4.** Plot of dislocation density versus grain-size. Xenolith data are plotted as black squares with  $1\sigma$  error bars. The solid black line represents the relationship between dislocation density and grain-size for olivine deforming in steady state. The gray band surrounding the black line represents the  $1\sigma$  uncertainty in the experimentally calibrated piezometers. Any data that plot above this line have likely experienced a stress pulse. Data that plot below this line have been subject to static annealing. The blue lines emanating from each data point are the paths that the samples would follow during static annealing. The red contours are annealing times. The stippled region is excluded; data may not fall in this region. All data plot very close to the black line, indicating that no postdeformational microstructural alteration has occurred. Furthermore, all data plot above the  $10^7$  s annealing contour, indicating that exhumation of the xenoliths occurred within  $10^7$  s of the cessation of deformation.

where  $A$  is a pre-exponential factor,  $E^*$  is the activation energy,  $V^*$  is the activation volume, and  $n$  is a constant. Although pressure effects are known to be important, there is still ongoing research that seeks to refine the magnitude of this effect. In Figure 5, we plot olivine strain rates for a conservative range of  $V^* = 10\text{--}20$  cm<sup>3</sup>/mol. The stress range, from 10–100 MPa, is a conservative estimate based on the piezometry discussed earlier. For  $V^* = 0$  cm<sup>3</sup>/mol, which roughly corresponds to the assumptions made by previous authors, olivine strain rates would be as high as  $5 \cdot 10^{-8}$ – $5 \cdot 10^{-5}$  s<sup>-1</sup>. For our preferred value of  $V^* = 14$  cm<sup>3</sup>/mol [Karato and Rubie, 1997; Karato and Jung, 2003], strain rates are much lower:  $1 \cdot 10^{-10}$ – $1 \cdot 10^{-7}$  s<sup>-1</sup>.

#### 4.4. Orthopyroxene Strain Rate

[21] The strain rate attained by the orthopyroxene is more difficult to constrain, as there is only limited experimental data on orthopyroxene rheology. Early deformation experiments on orthopyroxene are of limited utility because these works did not correct for the effect of friction in the load cell [Raleigh et al., 1971; Ross and Nielsen, 1978]. More recent experimental work in gas-medium apparatuses covered a limited range of pressures, and can barely attain the conditions of stability for orthoenstatite, the stable upper-mantle structure of orthopyroxene [Mackwell, 1991; Lawlis, 1998]. Lawlis [1998] conducted a few experiments at  $P = 450$  MPa, which were inferred to be in the orthoenstatite stability field. We will apply this flow-law in our study.

Ideally, we would like to use equation (2) for this analysis, however as  $V^*$  is unknown for orthopyroxene, we will use the homologous temperature to estimate the effects of pressure on deformation:

$$\dot{\epsilon} = A\sigma^n \exp\left(-\beta \frac{T_m(P)}{T}\right) \quad (3)$$

where  $\beta$  is a nondimensional constant and  $T_m$  is the melting temperature, calculated from the enstatite melting curve of Gasparik [1994]. This formulation, at  $P = 5.5$  GPa, roughly corresponds to  $V^* = 13$  cm<sup>3</sup>/mol.

[22] Because of the layered microstructure, we assume that the system is close to the constant stress bound. Therefore we assume that the stress applied during deformation is the same in orthopyroxene as in olivine. Applying the [Lawlis, 1998] orthoenstatite flow law, we estimate that the orthopyroxene porphyroclasts experienced strain rates of  $3 \cdot 10^{-12}$ – $3 \cdot 10^{-9}$  s<sup>-1</sup>, where the range of values again corresponds to the conservative range of stresses determined above (10–100 MPa). The orthopyroxene neoblasts, as demonstrated earlier, are not deforming by dislocation creep, but by a grain-size sensitive mechanism that is progressively randomizing the inherited fabric. As there have been no explicit rheological studies of grain-size sensitive creep in orthopyroxene to date, we will not attempt to calculate the strain rates achieved by the orthopyroxene neoblasts. However, because their deformation was presumably grain-size

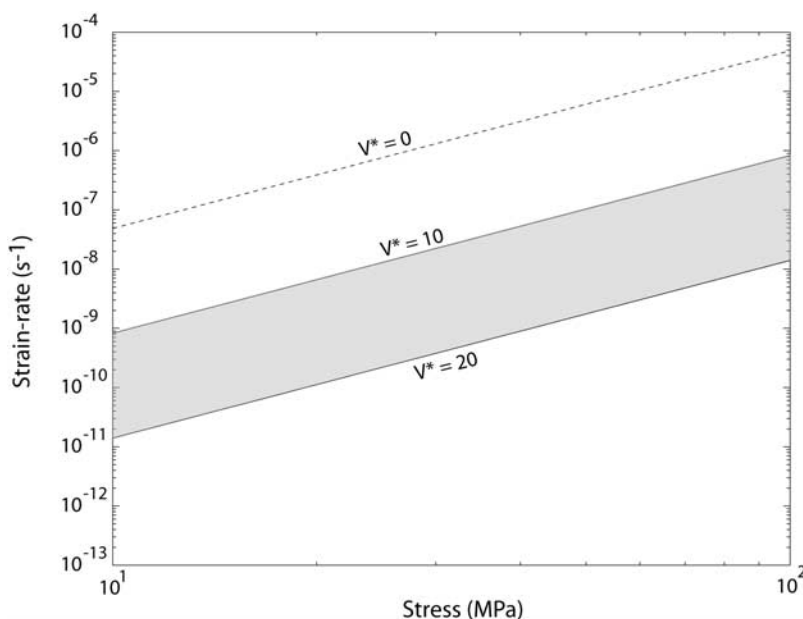


**Figure 5.** Olivine strain rate versus stress for a range of activation volumes.  $V^* = 0$  corresponds to the case where pressure effects are ignored.  $V^* = 10\text{--}20$  cm<sup>3</sup>/mol is more consistent with current experimental data.

sensitive, they must be rheologically weaker than the associated porphyroclasts [Rutter and Brodie, 1988].

#### 4.5. Geological Significance

[23] As we have just noted, the interpretation of the rheology of the sheared-lherzolites is not straightforward, as there are still significant gaps in our understanding of the rheology of mantle phases. While the strain rates achieved by the sheared lherzolite xenoliths will require refinement as rheological data improve, we can speculate about the origins of the xenoliths given what is known now. Previous studies determined strain rates as high as  $10^{-4}$  s<sup>-1</sup>; our estimates, which incorporate the effects of pressure among other things, are lower by as much as five or six orders of magnitude. Even with these revised estimates, the strain rates achieved by these xenoliths are extremely fast; too fast to be explained by the motion of continents, or probably even by narrow shear-zones associated with plate boundaries. One possibility is that the high-strain rate deformation could be driven by ascending plumes [cf. Green and Gueguen, 1974]. The velocity of mantle plumes may be orders of magnitude faster than the rates of plate motion, 1 m a year, by some estimates [e.g., Larsen and Yuen, 1997]. A plume head, interacting with the stiff rheological base of the continental lithosphere, could conceivably induce strain rates of  $10^{-9}$  s<sup>-1</sup>, if the deformation was accommodated over a zone of a few hundred meters. The association with a mantle plume would also explain the elevated temperatures seen in the xenoliths, the well-known “kink” in kimberlite geotherms [Boyd, 1973], as well as the particular geochemical re-enrichment features of these xenoliths [Kesson and Ringwood, 1989].

### 5. Dynamic Recrystallization

#### 5.1. Theoretical Framework

[24] As described earlier, there are a number of microstructural differences between olivine and orthopyroxene in

sheared lherzolite xenoliths. One very obvious difference is in the size of the olivine and orthopyroxene neoblasts: olivine neoblasts are at least a factor of five larger than orthopyroxene neoblasts. Another notable difference is the degree of recrystallization: olivine is completely recrystallized whereas the recrystallization of orthopyroxene is incomplete. In a recent experimental study we argued that the persistence of the small orthopyroxene neoblasts through geologic time may be attributable to extremely slow grain-growth kinetics [Skemer and Karato, 2007]. Differences in the grain growth kinetics of olivine and orthopyroxene may also contribute to the contrasting recrystallized grain-size and the contrasting degree of recrystallization observed in the sheared-lherzolite xenoliths. To test this hypothesis we will use the Avrami theory of recrystallization, coupled with microstructural observations and experimental data, to constrain the material-specific parameters that control the dynamic recrystallization process.

[25] In the Avrami theory of recrystallization (or phase transformation), the recrystallization process is governed by two microscopic parameters: the nucleation rate and the growth rate [Riedel and Karato, 1996; Karato, 2008]. In this generic model, nucleation includes any process that produces high-angle boundaries, including progressive subgrain rotation and grain-boundary bulging [e.g., Urai et al., 1986]. The rate at which these nuclei are formed is called the nucleation rate,  $I$ , and will depend on the rates of the specific atomic scale processes that occur during recrystallization. These nuclei will grow with a growth rate,  $G$ , to consume the remaining parent grains. The time ( $\tau$ ) required for most of a sample to be consumed by recrystallized grains is determined by the nucleation and growth rates as:

$$\tau = \left( \frac{B}{G^{p-1}I} \right)^{\frac{1}{p}} \quad (4)$$

where  $p$  and  $B$  are nondimensional constants related to the mode of nucleation and the completeness of recrystallization, respectively [Karato, 2008]. When recrystallization is complete there will be a statistical balance between

nucleation and impingement in such a way as to control the grain-size, leading to:

$$\delta = \left( \frac{B \cdot G}{I} \right)^{\frac{1}{p}} \quad (5)$$

The validity of these relationships has been studied numerically by Riedel and Karato [1996].

[26] Because  $\delta$  and  $\tau$  can be inferred from microstructural observations, we rearrange these equations to solve for the material-specific parameters  $G$  and  $I$ , which control the microstructural evolution.

$$G = \frac{\delta}{\tau} \quad (6)$$

$$I = \frac{B}{\tau \delta^{p-1}} \quad (7)$$

Given the lack of microstructural recovery in these samples,  $\delta_{ol}$  and  $\delta_{opx}$  are well constrained by the olivine and orthopyroxene recrystallized grain-sizes, respectively. Thus to determine  $G_{ol}$ ,  $G_{opx}$ ,  $I_{ol}$  and  $I_{opx}$ , we must determine  $\tau_{ol}$  and  $\tau_{opx}$ , which is the time required to dynamically recrystallize the olivine and orthopyroxene porphyroclasts. These timescales are more difficult to constrain, and will require some discussion.

[27] Orthopyroxene is largely recrystallized, so we will assume that the characteristic time for recrystallization is roughly comparable to the duration of deformation:

$$\tau_{opx} = \frac{\varepsilon_{opx}}{\dot{\varepsilon}_{opx}} \quad (8)$$

where  $\varepsilon$  is the finite shear strain and  $\dot{\varepsilon}$  is the shear strain rate.  $\dot{\varepsilon}_{opx}$  is calculated following the procedure outlined above.  $\varepsilon_{opx}$  can be crudely estimated from the shape of the recrystallized domains, by assuming that the initial shape of the unrecrystallized domain was spherical [cf. Gueguen and Boullier, 1976]. For the recrystallized bands shown in Figure 3,  $\varepsilon \sim 5$ . This is likely a lower bound, however, since the orthopyroxene bands are often interconnected, obscuring the maximum degree of strain. The calculations shown in Figure 6 assume  $\varepsilon_{opx} = 10$ .

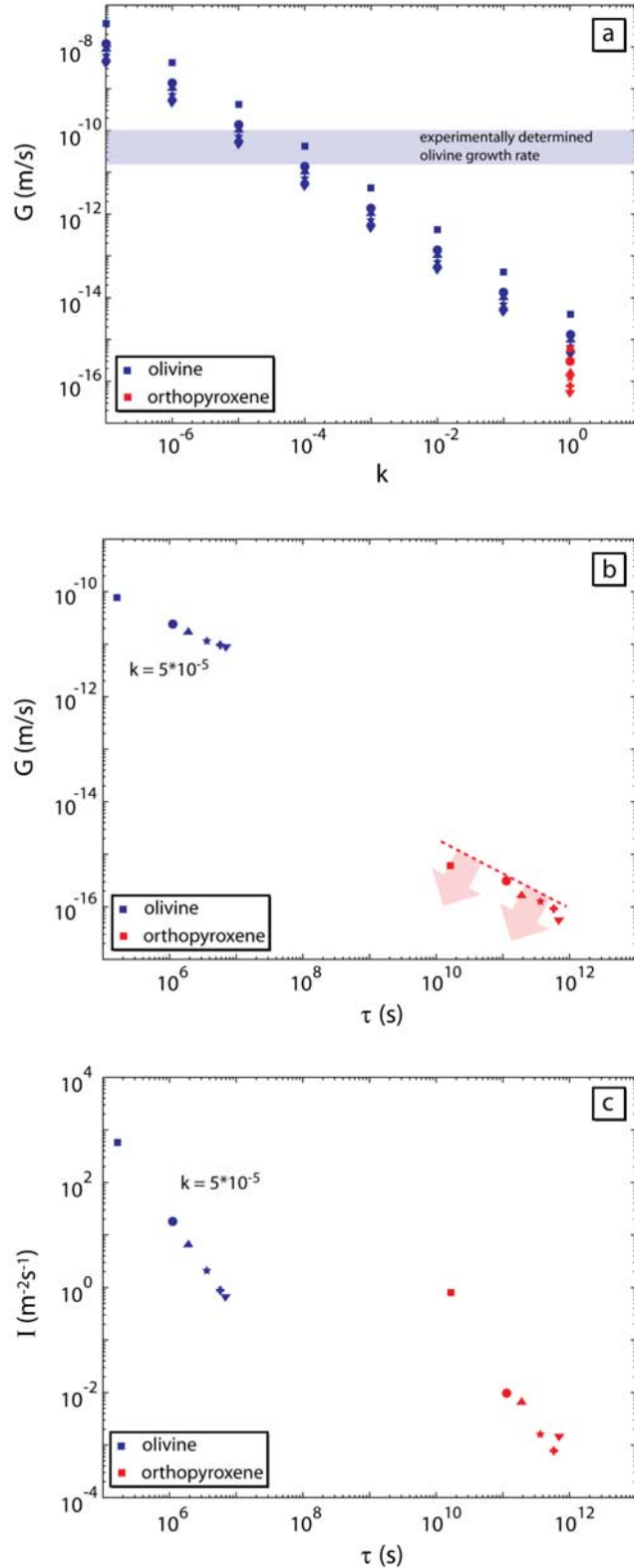


**Figure 6.** (a) Growth-rate ( $G$ ) as a function of  $k$ . Olivine is plotted as blue symbols. Orthopyroxene is plotted as red symbols. Each symbol shape corresponds to an individual sample from Table 1. For orthopyroxene,  $k = 1$  by definition. For olivine,  $k$  is unknown, so  $G_{ol}$  is plotted for  $k = 10^0 - 10^{-7}$ . An independent, experimentally constrained value for olivine growth rate is plotted as the blue band. This band intersects  $G_{ol}$  calculated from Avrami theory at  $k \sim 5 \cdot 10^{-5}$ . (b) Growth rate ( $G$ ) as a function of recrystallization time ( $\tau$ ), illustrating the contrast in both between olivine and orthopyroxene. The dashed red line represents a microstructurally constrained upper limit to the growth rate of orthopyroxene, based on the absence of observed secondary recrystallization in these samples. (c) Nucleation rate ( $I$ ) as a function of recrystallization time ( $\tau$ ), calculated assuming grain-boundary nucleation.

[28] Olivine, on the other hand, is completely recrystallized, so  $\tau_{ol}$  must be some factor less than  $\tau_{opx}$ . Without any further microstructural observations to constrain  $\tau_{ol}$ , we simply define the characteristic time for the recrystallization of olivine as:

$$\tau_{ol} = k\tau_{opx} \quad (9)$$

where  $k$  is an unknown, nondimensional constant that ranges from 0 to 1.

## 5.2. Growth Rates

[29] Figure 6a shows  $G_{opx}$  and  $G_{ol}$  calculated from equation (6). For the six samples listed in Table 1,  $G_{opx}$  ranges from  $4*10^{-17}$ – $5*10^{-16}$  m/s.  $G_{ol}$  is calculated for a large range of  $k$  ( $10^0$ – $10^{-7}$ ) and is not well constrained by this analysis. To provide a better constraint on  $G_{ol}$  and also determine a reasonable value for  $k$ , we require an independent estimate of olivine growth rates.

[30] An independent estimate of olivine growth rates can be readily derived from experimental data on the kinetics of static or secondary grain-growth in olivine. In this formulation, the velocity of grain boundary migration ( $G$ ) is treated as the product of the grain-boundary mobility ( $M$ ) and a driving force ( $F$ ):

$$G = MF \quad (10)$$

Grain-boundary mobility is a material-specific property that depends on temperature and pressure through an Arrhenius-type relationship. At 1623 K and 5.5 GPa dry olivine grain-boundary mobility is experimentally determined to be  $\sim 1*10^{-14}$   $\text{ms}^{-1}\text{Pa}^{-1}$  [Karato, 1989]. The driving force for grain boundary migration during primary recrystallization is likely the contrast in dislocation density between the recrystallizing porphyroclast and the initially strain-free neoblast [e.g., Urai *et al.*, 1986]:

$$F = \mu b^2 \Delta\rho \quad (11)$$

Where  $\mu$  is the shear modulus,  $b$  is the length of the Burgers vector, and  $\Delta\rho$  is the difference in dislocation density between the porphyroclast and the neoblast. For dislocation densities of  $1$ – $5*10^{11}$   $\text{m}^{-2}$ , the driving force for grain-growth is  $F \sim 2$ – $10$   $\text{kJ/m}^3$ . Olivine growth rates calculated in this manner are plotted as the blue band in Figure 6a; these growth rates are roughly five orders of magnitude faster than the calculated values for  $G_{opx}$ . Olivine growth rates calculated from the Avrami theory intersect this band at  $k \sim 5*10^{-5}$ . Therefore we conclude that  $k = 5*10^{-5}$  represents the contrast in the characteristic times for the recrystallization of olivine and orthopyroxene (Figure 6b).

[31] Using further microstructural considerations, we can independently constrain the orthopyroxene growth-rate calculation. As we demonstrated earlier, after their formation the orthopyroxene neoblasts deformed by a grain-size sensitive mechanism. In the absence of ongoing dislocation creep, it is expected that the orthopyroxene neoblasts should have undergone quasi-static (secondary) grain-growth. However, there is no perceptible evidence of grain-growth from the newest to the oldest neoblasts (Figure 3). We can

use the absence of secondary grain-growth to provide a fairly robust upper limit to the rate of primary grain-growth. If we assume, conservatively, that a factor of 2 increase in grain-size is needed to be perceptible beyond the margins of error, and that primary grain-growth is driven by the reduction of grain-boundary energy, an upper limit for orthopyroxene grain-boundary mobility can be calculated as [cf. Skemer and Karato, 2007]:

$$M \leq \frac{3\delta^2}{\tau A \gamma} \quad (12)$$

where  $\delta$  is the observed grain-size, the grain-growth exponent is assumed to be 2 [e.g., Atkinson, 1988],  $A$  is a nondimensional constant of order 0.5,  $\gamma$  is the grain boundary energy (of order 1  $\text{J/m}^2$ ), and  $\tau$  is the duration of deformation, as calculated above. The upper limit for orthopyroxene grain-boundary mobility, calculated in this manner for the six samples listed in Table 1, is  $\sim 1$ – $5*10^{-20}$   $\text{ms}^{-1}\text{Pa}^{-1}$ . Multiplying these values for mobility by the driving force for primary grain growth (equation (11), assuming dislocation densities in olivine and orthopyroxene are comparable), we get an upper limit for the primary growth rate of the orthopyroxene neoblasts. This upper limit is plotted as a dashed red line on Figure 6b. The orthopyroxene growth rates calculated from Avrami theory fall below this upper limit, indicating that the two results are consistent.

## 5.3. Nucleation Rates

[32] Figure 6c shows values for the nucleation rate  $I_{opx}$  and  $I_{ol}$  calculated using equation (7). Nucleation in orthopyroxene is observed to occur almost exclusively on grain boundaries. Therefore in this calculation we assume  $p = 3$  [Karato, 2008].  $B$ , as noted earlier, is a constant related to the completeness of recrystallization. Although the degrees of recrystallization are different for olivine and orthopyroxene, we will analyze both data sets assuming recrystallization is 75% complete ( $B = 1.4$ ), allowing us to directly compare the calculated nucleation rates. For the samples listed in Table 1,  $I_{opx}$  ranges from  $7*10^{-4}$ – $8*10^{-1}$   $\text{m}^{-2}\text{s}^{-1}$ . For our preferred value for  $k$  ( $5*10^{-5}$ ),  $I_{ol}$  ranges from  $5*10^{-1}$ – $5*10^2$ . Thus nucleation rates in olivine are about three orders of magnitude faster than nucleation rates in orthopyroxene.

## 5.4. Contributions of Growth Rate and Nucleation Rate to Microstructural Development

[33] To summarize, the Avrami theory of recrystallization prescribes that recrystallized grain-size ( $\delta$ ) and the timescale for recrystallization ( $\tau$ ) should depend on both a growth rate ( $G$ ) and a nucleation rate ( $I$ ). Given this theory and additional experimental constraints, we find that  $G_{ol}$  is roughly five orders of magnitude faster than  $G_{opx}$ . Olivine nucleation rates are also faster than orthopyroxene nucleation rates, but by about three orders of magnitude. While both of these effects are clearly important, we conclude that the contrast in grain-growth rate plays the larger role in influencing microstructural development of the sheared lherzolite xenoliths. The uncertainties in this calculation are largely contained in the determination of the recrystallization time ( $\tau$ ), as the finite strain of orthopyroxene is not

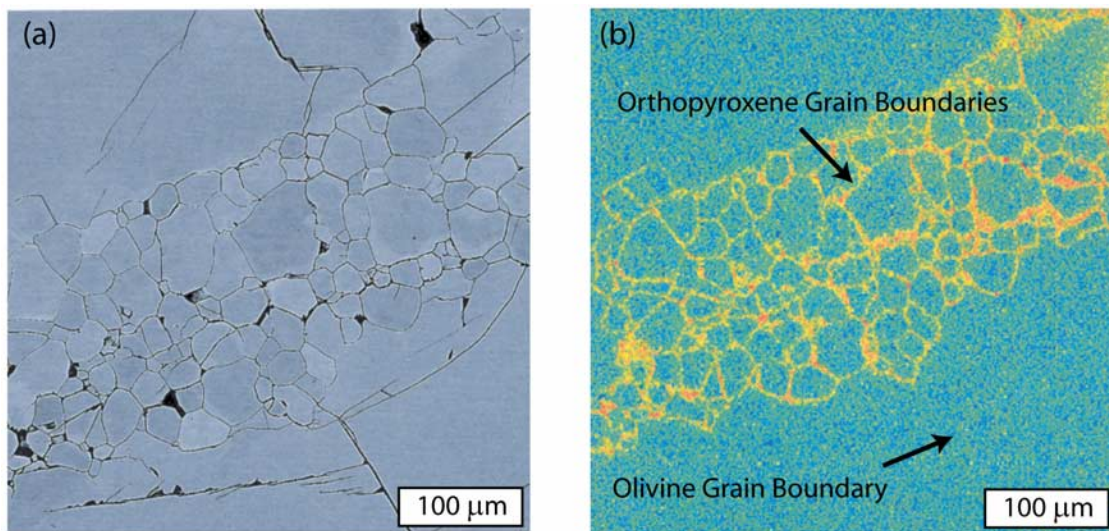


**Figure 7.** (a) SEM image of a band of recrystallized orthopyroxene, surrounded on both sides by olivine. (b) X-ray chemical map of aluminum. Orthopyroxene grain boundaries and orthopyroxene-olivine phase boundaries are enriched in aluminum, while olivine grain boundaries do not show any evidence of enrichment. While the apparent width of the enriched layer is on the order of a micron, this may be an artifact of the spatial resolution of the analytical technique, which is also roughly a micron.

well constrained. However, since both  $G$  and  $I$  are inversely proportional to  $\tau$ , the uncertainties will effect both in the same manner.

## 6. Summary and Conclusions

[34] Sheared lherzolite xenoliths are geologically enigmatic samples, but valuable as a natural laboratory for the study of large strain, high temperature and high pressure deformation of peridotite. In this study we have demonstrated that deformation in these xenoliths is manifested very differently in olivine and orthopyroxene. At these particular deformation conditions olivine recrystallizes rapidly and all subsequent deformation is in the dislocation creep regime. Orthopyroxene, on the other hand, recrystallizes more slowly, the neoblasts are much smaller, and all subsequent deformation is in a grain-size sensitive regime. These observations indicate that transient deformation phenomena persist longer in orthopyroxene than in olivine. Using the Avrami theory of recrystallization, coupled with microstructural and experimental constraints, we conclude that these microstructural differences are largely attributable to differences in the relative rates of grain-boundary migration, as well as differences in rate of neoblast nucleation.

[35] This conclusion is supported by recent experimental work, which demonstrated that static grain-growth in orthopyroxene is extremely slow in comparison to olivine [Skemer and Karato, 2007]. In this experimental study, we argued that grain-boundary migration in orthopyroxene is inhibited by the presence of cations segregated on and near grain-boundaries, a phenomenon referred to as impurity drag [e.g., Yan *et al.*, 1977]. Olivine, which can only dissolve small quantities of impurities, is largely unaffected by this process. Indeed, high resolution X-ray mapping of the sheared-lherzolite xenoliths shows aluminum enrichment along orthopyroxene grain boundaries but not along

olivine grain boundaries (Figure 7). The absence of enrichment along the olivine grain-boundaries suggests that the enrichment on the orthopyroxene grain boundaries is not of metasomatic origins. However, we cannot exclude the possibility that this enrichment is associated with partial chemical re-equilibration during exhumation.

[36] These microstructural observations have broad significance, because they indicate that the rheology of peridotite may be influenced significantly by differences in the recrystallization behavior of olivine and orthopyroxene. Specifically, the slow kinetics of orthopyroxene grain-boundary migration influence deformation in a number of ways: (1) The rate of recrystallization is slower in orthopyroxene than in olivine, which means that a steady state microstructure takes longer to develop. (2) The recrystallized grain size is small, which can lead to a transition from dislocation creep to grain-size sensitive creep. (3) Deformation in this grain-size sensitive state can persist long enough to accumulate large strains. (4) Highly deformed peridotites like the sheared lherzolite xenoliths may remain microstructurally weak long after the initial high-stress deformation event has ceased.

[37] One of the weaknesses of the present analysis is the limited experimental data on the rheology of orthopyroxene. Improved rheological data will allow us to calculate an orthopyroxene deformation mechanism map [e.g., Frost and Ashby, 1982], which will in turn allow us to predict (1) the range of conditions where orthopyroxene may deform by grain-size sensitive mechanisms, (2) how much weakening might occur, and (3) how long deformation in this weakened state might persist.

[38] In conclusion, we suggest that to fully understand the deformation of the upper mantle, particularly in highly deformed regions like plate boundaries, we must not overlook the importance of orthopyroxene. The sluggish kinetics of grain-boundary migration has a dramatic influence on

microstructural evolution, and may permit long-term deformation in a grain-size sensitive, weakened rheological state. Experimental studies on the rheological behavior of orthopyroxene will greatly improve our understanding of the geological significance of these phenomena, and as such will have profound implications for our understanding of Earth.

[39] **Acknowledgments.** The authors gratefully acknowledge the donation of samples by Joe Boyd. Zhenting Jiang is thanked for his assistance with EBSD. Masaru Takakura at JEOL-Japan is thanked for his assistance with high-resolution FEG-EPMA composition measurements. David Prior and two anonymous reviewers are thanked for their helpful comments. This work was supported by NSF EAR-0309448.

## References

- Atkinson, H. (1988), Theories of normal grain growth in pure single phase systems, *Acta Metal.*, 36(3), 469–491.
- Avrami, M. (1939), Kinetics of phase change. Part I: General theory, *J. Chem. Phys.*, 7, 1105–1112.
- Bestmann, M., and D. J. Prior (2003), Intragranular dynamic recrystallization in naturally deformed calcite marble: Diffusion accommodated grain boundary sliding as a result of subgrain rotation recrystallization, *J. Struct. Geol.*, 25(10), 1597–1613.
- Boullier, A. M., and Y. Gueguen (1975), SP-mylonites: Origin of some mylonites by superplastic flow, *Contrib. Mineral. Petrol.*, 50(2), 93–104.
- Boullier, A. M., and A. Nicolas (1975), Classification of textures and fabrics of peridotite xenoliths from South African kimberlites, *Phys. Chem. Earth*, 9, 467–475 (First international conference on Kimberlites).
- Boyd, F. R. (1973), A pyroxene geotherm, *Geochim. Cosmochim. Acta*, 37(12), 2533–2546.
- Boyd, F. R., and S. A. Mertzman (1987), Composition and structure of the Kaapvaal lithosphere, Southern Africa, in *Magmatic Processes; Physicochemical Principles; A Volume in Honor of Hatten S. Yoder Jr.*, edited by B. O. Mysen, pp. 13–24, Geochemical Society, Univ. Park, Pa.
- Boyd, F. R., and P. H. Nixon (1975), Origins of the ultramafic nodules from some kimberlites of northern Lesotho and the Monastery Mine, South Africa, *Phys. Chem. Earth*, 9, 431–454 (First international conference on kimberlites).
- Brey, G. P., and T. Koehler (1990), Geothermobarometry in four-phase lherzolites. Part II: New thermobarometers, and practical assessment of existing thermobarometers, *J. Petrol.*, 31(6), 1353–1378.
- Chopra, P. N., and M. S. Paterson (1984), The role of water in the deformation of dunite, *J. Geophys. Res.*, 89, 7861–7876.
- Christensen, N. L., and S. M. Lundquist (1982), Pyroxene orientation within the upper mantle, *Geol. Soc. Am. Bull.*, 93(4), 279–288.
- de Bresser, J. H. P., et al. (1998), On dynamic recrystallization during solid state flow: Effects of stress and temperature, *Geophys. Res. Lett.*, 25(18), 3457–3460.
- de Bresser, J. H. P., et al. (2001), Grain size reduction by dynamic recrystallization; Can it result in major rheological weakening?, in *Deformation Mechanisms, Rheology and Microstructures*, edited by G. Dresen and M. Handy, Springer, Berlin.
- Durham, W. B., et al. (1977), Plastic flow of oriented single crystals of olivine: 2. Observations and interpretations of the dislocation structures, *J. Geophys. Res.*, 82(36), 5755–5770.
- Ehrenberg, S. N. (1979), Garnetiferous ultramafic inclusions in minette from the Navajo volcanic field, in *The Mantle Sample; Inclusions in Kimberlites and Other Volcanics*, edited by F. R. Boyd and H. O. A. Meyer, pp. 330–344, AGU, Washington, D. C.
- Fliervoet, T. F., et al. (1999), Crystallographic preferred orientations and misorientations in some olivine rocks deformed by diffusion or dislocation creep, in *Deformation Mechanisms in Nature and Experiment*, edited by S. M. Schmid et al., pp. 1–27, Elsevier, Amsterdam.
- Frost, H., and M. Ashby (1982), *Deformation-Mechanism Maps: The Plasticity and Creep of Metals and Ceramics*, 1st ed., Elsevier, New York.
- Gasparik, T. (1994), Experimentally determined melting relations in simple and complex chemical systems at pressures up to 23 GPa, in *V. M. Goldschmidt Conference; Extended Abstracts*, edited by B. Harte, pp. 321–322, Mineralogical Society, London.
- Goetze, C. (1975), Sheared lherzolites: From the point of view of rock mechanics, *Geology*, 3(4), 172–173.
- Gomez Barreiro, J., et al. (2007), Preferred orientation of anorthite deformed experimentally in Newtonian creep, *Earth Planet. Sci. Lett.*, 264, 188–207.
- Green, H. W., II, and Y. Gueguen (1974), Origin of kimberlite pipes by diapiric upwelling in the upper mantle, *Nature*, 249(5458), 617–620.
- Gueguen, Y., and A. M. Boullier (1976), Evidence of superplasticity in mantle peridotites, in *The Physics and Chemistry of Minerals and Rocks*, edited by R. G. J. Strens, pp. 19–33, John Wiley, London.
- Halfpenny, A., et al. (2006), Analysis of dynamic recrystallization and nucleation in a quartzite mylonite, *Tectonophysics*, 427(1–4), 3–14.
- Hirth, G., and D. L. Kohlstedt (2003), Rheology of the upper mantle and the mantle wedge: A view from the experimentalists, in *Inside the Subduction Factory*, edited, pp. 83–105, AGU, Washington D. C.
- Huebner, J. S., and D. E. Voigt (1984), Chemical diffusion in Ca-Mg-Fe pyroxenes; Measured rates of cation exchange and interface movement, in *The Geological Society of America, 97th Meeting*, edited, 546 pp., Geol. Soc. Am., Boulder, Colo.
- Jin, D. (1995), Deformation microstructures of some ultramafic rocks, Masters thesis, 115 pp., Univ. of Minn., Minneapolis, Minnesota.
- Jung, H., and S.-i. Karato (2001a), Water-induced fabric transitions in olivine, *Science*, 293(5534), 1460–1462.
- Jung, H., and S.-i. Karato (2001b), Effects of water on dynamically recrystallized grain-size of olivine, *J. Struct. Geol.*, 23(9), 1337–1344.
- Karato, S. (1987), Scanning electron microscope observation of dislocations in olivine, *Phys. Chem. Miner.*, 14(3), 245–248.
- Karato, S. (1989), Grain growth kinetics in olivine aggregates, *Tectonophysics*, 168(4), 255–273.
- Karato, S.-i. (2008), *Deformation of Earth Materials*, 562 pp., Cambridge Univ., New York.
- Karato, S., and H. Jung (2003), Effects of pressure on high-temperature dislocation creep in olivine, *Philos. Mag. A and B*, 83(3), 401–414.
- Karato, S. i., and M. Ogawa (1982), High-pressure recovery of olivine; implications for creep mechanisms and creep activation volume, *Phys. Earth Planet. Inter.*, 28(2), 102–117.
- Karato, S. i., and D. C. Rubie (1997), Toward an experimental study of deep mantle rheology; a new multi-anvil sample assembly for deformation studies under high pressures and temperatures, *J. Geophys. Res.*, 102(9), 20,111–20,122.
- Karato, S., and P. Wu (1993), Rheology of the upper mantle: A synthesis, *Science*, 260, 771–777.
- Karato, S. i., et al. (1980), Dynamic recrystallization of olivine single crystals during high-temperature creep, *Geophys. Res. Lett.*, 7(9), 649–652.
- Karato, S., et al. (1995), Superplasticity in Earth's lower mantle - Evidence from seismic anisotropy and rock physics, *Science*, 270(5235), 458–461.
- Katayama, I., et al. (2004), New type of olivine fabric from deformation experiments at modest water content and low stress, *Geology*, 32(12), 1045–1048.
- Kennedy, L. A., et al. (2002), Mantle shear zones revisited; the connection between the cratons and mantle dynamics, *Geology*, 30(5), 419–422.
- Kesson, S. E., and A. E. Ringwood (1989), Slab-mantle interactions. Part I: Sheared and refertilised garnet peridotite xenoliths; Samples of Wadati-Benioff zones?, *Chem. Geol.*, 78(2), 83–96.
- Kohlstedt, D. L., and C. Goetze (1974), Low-stress high-temperature creep in olivine single crystals, *J. Geophys. Res.*, 79(14), 2045–2051.
- Larsen, T. B., and D. A. Yuen (1997), Ultrafast upwelling bursting through the upper mantle, *Earth Planet. Sci. Lett.*, 146(3–4), 393–399.
- Lawlis, J. (1998), High temperature creep of synthetic olivine-enstatite aggregates, Ph.D. thesis, 132 pp., Pennsylvania State Univ., State College Pennsylvania.
- Mackwell, S. J. (1991), High-temperature rheology of enstatite; implications for creep in the mantle, *Geophys. Res. Lett.*, 18(11), 2027–2030.
- Mei, S., and D. L. Kohlstedt (2000), Influence of water on plastic deformation of olivine aggregates: 2. Dislocation creep regime, *J. Geophys. Res.*, 105(B9), 21,471–21,481.
- Mercier, J. C. C. (1979), Peridotite xenoliths and the dynamics of kimberlite intrusion, in *The Mantle Sample; Inclusions in Kimberlites and Other Volcanics*, edited by F. R. Boyd and H. O. A. Meyer, pp. 197–212, AGU, Washington, D. C.
- Mercier, J. C., and A. Nicolas (1975), Textures and fabrics of upper-mantle peridotites as illustrated by xenoliths from basalts, *J. Petrol.*, 16(2), 454–487.
- Mercier, J. C., et al. (1977), Stress in the lithosphere; inferences from steady state flow of rocks, *Pure Appl. Geophys.*, 115(1–2), 199–226, (Stress in the Earth).
- Nicolas, A., et al. (1971), Textures, structures and fabrics due to solid state flow in some European lherzolites, *Tectonophysics*, 12(1), 55–86.
- Nixon, P., et al. (1973), The evidence of kimberlite and its inclusion on the constitution of the outer part of the Earth, in *Lesotho Kimberlites*, edited by P. Nixon, pp. 312–318, Lesotho Natl. Dev. Corp., Maseru, Lesotho.
- Passchier, C., and R. Trouw (1998), *Microtectonics*, 289 pp., Springer, New York.
- Paterson, M. S. (1982), The determination of hydroxyl by infrared absorption in quartz, silicate glasses and similar materials, *Bull. Miner.*, 105(1), 20–29.

- Poirier, J. P. (1985), *Creep of Crystals*, Cambridge Univ. Press, New York.
- Post, R. L., and D. T. Griggs (1973), The Earth's mantle: Evidence of non-Newtonian flow, *Science*, *181*, 1242–1244.
- Raleigh, C. B., et al. (1971), Slip and the clinostatite transformation as competing rate processes in enstatite, *J. Geophys. Res.*, *76*(17), 4011–4022.
- Randle, V. (2003), *Microtexture Determination and Its Applications*, 2nd ed., 138 pp., Maney for the Institute of Materials, Minerals and Mining, London.
- Riedel, M. R., and S. Karato (1996), Microstructural development during nucleation and growth, *Geophys. J. Int.*, *125*, 397–414.
- Ross, J. V., and K. C. Nielsen (1978), High-temperature flow of wet polycrystalline enstatite, *Tectonophysics*, *44*(1–4), 233–261.
- Ross, J. V., et al. (1980), Stress dependence of recrystallized-grain and subgrain size in olivine, *Tectonophysics*, *70*(1–2), 39–61.
- Rutter, E. H., and K. H. Brodie (1988), The role of tectonic grain size reduction in the rheological stratification of the lithosphere, in *Detachment and Shear*, edited by H. Zankl et al., pp. 295–308, Springer, Berlin.
- Rutter, E. H., et al. (1994), Preferred crystallographic orientation development during the plastic and superplastic flow of calcite rocks, *J. Struct. Geol.*, *16*(10), 1431–1446.
- Skemer, P., and S. I. Karato (2007), Effects of solute segregation on the grain-growth kinetics of orthopyroxene with implications for the deformation of the upper mantle, *Phys. Earth Planet. Inter.*, *164*(3–4), 186–196.
- Skemer, P., et al. (2005), The misorientation index: Development of a new method for calculating the strength of lattice-preferred orientation, *Tectonophysics*, *411*, 157–167.
- Storey, C. D., and D. J. Prior (2005), Plastic deformation and recrystallization of garnet: A mechanism to facilitate diffusion creep, *J. Petrol.*, *46*(12), 2593–2613.
- Toriumi, M., and S. Karato (1978), Experimental studies on the recovery process of deformed olivines and the mechanical state of the upper mantle, *Tectonophysics*, *49*(1–2), 79–95.
- Twiss, R. J. (1976), Structural superplastic creep and linear viscosity in the Earth's mantle, *Earth Planet. Sci. Lett.*, *33*(1), 86–100.
- Urai, J. L., et al. (1986), Dynamic recrystallization of minerals, in *Mineral and Rock Deformation; Laboratory Studies; The Paterson Volume*, edited by B. E. Hobbs and H. C. Heard, pp. 161–199, AGU, Washington, D. C.
- van der Wal, D., et al. (1993), Relationships between dynamically recrystallized grain size and deformation conditions in experimentally deformed olivine rocks, *Geophys. Res. Lett.*, *20*(14), 1479–1482.
- Warren, J. M., and G. Hirth (2006), Grain size sensitive deformation mechanisms in naturally deformed peridotites, *Earth Planet. Sci. Lett.*, *248*(1–2), 438–450.
- Wheeler, J., et al. (2001), The petrological significance of misorientations between grains, *Contrib. Mineral. Petrol.*, *141*, 109–124.
- Yan, M., R. M. Cannon, H. K. Bowen (1977), Grain boundary migration in ceramics, in *Ceramic Microstructures*, edited by R. Fulrath and J. A. Pask, pp. 276–307, Westview, Boulder, Colo.

---

S.-i. Karato, Department of Geology and Geophysics, Yale University, PO Box 208109, New Haven, CT 06520-8109, USA.

P. Skemer, Department of Geosciences, Brown University, PO Box 1846, Providence, RI 02912, USA. (philip\_skemer@brown.edu)